Pole-zero diagram approach to the design of ring resonator-basedfilters for photonic applications

Author:
Kaalund, Christopher; Peng, Gang-Ding

Publication details:
Journal of Lightwave Technology
v. 22
Chapter No. 6
pp. 1548-1559
0733-8724 (ISSN)

Publication Date:
2004

Publisher DOI:
http://dx.doi.org/10.1109/JLT.2004.824526

Pole-Zero Diagram Approach to the Design of Ring Resonator-Based Filters for Photonic Applications

Christopher J. Kaalund and Gang-Ding Peng

***Abstract*—The pole-zero diagram is a tool that has been widely employed in digital and electronic filter design. It greatly facilitates filter design by producing a simple and direct visualization of parametrical behaviors and general spectral characteristics. In this paper, we propose new methods of applying pole-zero diagrams to photonic filter design, aimed at tailoring spectral characteristics. In particular, we demonstrate the effectiveness of this method in designing ring resonator-based filters for application to optical wavelength interleavers and deinterleavers. We show that there exist close relations between the pole-zero diagram of an optical filter and its wavelength response, and derive pole-zero diagrams for filters with various ring resonator configurations. Further, we propose a novel graphical technique using pole-zero diagrams for optimizing filter performance. As a practical example to demonstrate the effectiveness of the pole-zero approach, we present a new wavelength interleaver design with low crosstalk. This design was realized by superimposing the pole-zero diagrams of parallel and series-coupled ring resonator arrays.**

***Index Terms*—Integrated optics, optical planar waveguide components, optical waveguide filters, resonator filters.**

I. Introduction

VARIOUS photonic components, such as add–drop multiplexers and interleavers, are important in wavelength-division-multiplexed (WDM) fiber-optic networks. The growing complexity of these systems is driving demand for photonic components with lower cost, smaller footprint, lower power dissipation, and, in particular, sophisticated spectral or wavelength properties. One type of structure for photonic components is the optical ring resonator. Ring resonators can be used to construct various passive or active components in the form of fiber or planar waveguide. In planar waveguide form, ring resonators range in size from several micrometers to hundreds of micrometers, and can be cascaded or suitably configured to tailor the spectral response and other relevant characteristics. Previously, highly compact photonic components based on planar waveguide ring resonators have been fabricated for applications such as add–drop multiplexing [1], [2] and switching [3].

Ring resonators, together with Mach–Zehnder interferometers (MZIs), are fundamental building blocks for the construction of optical filters. A detailed analysis of these types of filters has been done in [4], which employed the Z-transform to calculate spectral and temporal response. Reference [4] presents sophisticated algorithms for optimizing MZI and ring resonator arrays for bandpass, gain equalizing, and dispersion compensating filters.

The spectral response of an optical filter based on MZIs and ring resonators is usually derived from a transfer function, calculated with the aid of the Z-transform. The transfer function generally has a very complex dependence on various device parameters, such as resonance frequencies and coupling coefficients. Inspection of this function usually provides no clues for optimizing a design. Further, the sophisticated synthesis methods that have been developed for certain filter configurations, such as in [4], are generally not applicable or easily adaptable to other filter types or design objectives. However, Z-transforms can be graphically represented using pole-zero diagrams [4]–[9]. As we shall show, pole-zero diagrams allow complex parametrical dependencies to be clearly visualized. This suggests a simple graphical method of using pole-zero diagrams to compare different filter configurations and optimize their performance through manipulating the positions of poles and zeros. In this paper, we present methods for adjusting spectral response based on pole-zero diagrams to optimize spectral characteristics such as crosstalk and passband shape.

To illustrate the use of pole-zero diagrams, we apply them in this paper to the design of a wavelength interleaver. [10]–[12] Wavelength interleavers combine two separate streams of channels into one stream with half the channel spacing, and deinterleavers perform the opposite function. They can be produced using cascaded MZIs [10] and ring resonators [11], [12] in various configurations. In this paper we use pole-zero diagrams to predict the performance of various interleavers designs.

This paper proposes the use of pole-zero diagrams for the design and optimization of filters for photonics applications. We studied, compared, and optimized various filter structures for wavelength interleaving. Starting with the known and simple cases for interleavers proposed previously, we demonstrate that the pole-zero diagram method proposed in this paper provides insights that are difficult to ascertain using previous methods based only on calculation of the spectrum in terms of a transfer function. Close relations between the pole-zero diagram features of a ring resonator-based filter and its spectral response were observed. Further, we summarize a graphical technique based on pole-zero diagrams for photonic filter design and optimization. As far as we know, this design technique is novel and has not been previously proposed in the literature. Finally, we used the pole-zero diagram method to produce a new design of wavelength interleaver consisting of both parallel and series-coupled ring resonator filter arrays.

Manuscript received June 18, 2003; revised December 22, 2003.

The authors are with the Photonics and Optical Communications Group, School of Electrical Engineering and Telecommunications, The University of New South Wales, 2052 Sydney, Australia.

Digital Object Identifier 10.1109/JLT.2004.824526

II. Pole-Zero Diagrams

A. Theory of Pole-Zero Diagrams

In this section we explain pole-zero diagrams and relate them to filter spectral response. The optical filters that we discuss in this paper have periodic spectral responses. It is well known in the field of digital signal processing that discrete time signals have periodic spectra [5]. Therefore, it is appropriate to represent periodic optical spectra as discrete sequences. Given the additional constraints of linearity and time invariance, it can be shown that a filter's time response is completely characterized by a discrete impulse response function, which we denote $h(n)$ [5]. The index n is a discrete time variable.

The frequency response of a filter can be derived from the Z-transform, which is a generalization of the Fourier transform for discrete time systems. Z-transforms are discussed extensively in many books on digital signal processing, such as [5]; however, we shall introduce them briefly. The Z-transform converts a discrete time signal into a complex-variable frequency signal via

$$H(z) = \sum_{n=-\infty}^{\infty} h(n) z^{-n}. \tag{1}$$

Here, z is a complex variable. Each term in this equation represents a delay, with z^{-1} corresponding to a unit delay, z^{-2} corresponding to twice this, and so on. For a causal filter, in which the output signal at time $n = n_0$ depends only on input values for which $n \leq n_0$, the summation begins at $n = 0$.

For a linear discrete system with input signal x, the output signal is

$$\begin{aligned} y(n) = {} & b_0 x(n) + b_1 x(n-1) + \ldots + b_M x(n-M) \\ & - a_1 y(n-1) - \ldots - a_N y(n-N). \end{aligned} \tag{2}$$

Comparing (1) and (2), it is evident that the Z-transform for this filter is

$$H(z) = \frac{\sum_{m=0}^{M} b_m z^{-m}}{1 + \sum_{n=1}^{N} a_n z^{-n}}. \tag{3}$$

The numerator and denominator can be factored to give the zeros z_m and poles p_n, respectively, as follows:

$$H(z) = \frac{\Gamma z^{N-M} \prod_{m=1}^{M} (z - z_m)}{\prod_{n=1}^{N} (z - p_n)}. \tag{4}$$

A pole-zero diagram is a graph of pole and zero positions on the complex z-plane. In this diagram, the linear frequency axis of the periodic spectrum is mapped to the unit circle in the complex plane. That is, z is related to the signal frequency ω by setting $z^{-1} = e^{-i\omega}$, thereby restricting z to the unit circle. $z = 1$ corresponds to $\omega = 0, \pm 2\pi, \pm 4\pi, \ldots$ and $z = -1$ corresponds to $\omega = \pm\pi, \pm 3\pi, \pm 5\pi, \ldots$. In the case of ring resonator filters, $z = 1$ corresponds to resonant frequencies. A complete circuit of the unit circle corresponds to the free spectral range (FSR) of the filter.

Poles and zeros are related to the frequency spectrum by their position on the complex plane. A zero positioned on the unit circle results in zero transmission at the frequency corresponding to the angle of that zero. Likewise, a pole on the unit circle will cause unity transmission at the corresponding frequency. As poles and zeros move away from the unit circle, their effect on the magnitude spectrum diminishes. Figs. 1 and 2 show how the magnitude spectra of single poles and zeros change as their distance from the unit circle varies. The frequency scale is normalized, with zero corresponding to the resonance frequency and one corresponding to half the FSR. Also note that the outermost circle for all pole-zero diagrams in this paper corresponds to the unit circle. Magnitude spectra with flatter passbands and lower crosstalk can be synthesized by adding poles and zeros at various locations on the complex plane. This is discussed in detail in [4].

By using planar waveguide MZIs and ring resonators, filters with arbitrary or approximate pole and zero positions can be produced. Coherent light that is launched into a waveguide traverses multiple MZI and ring resonator stages, resulting in transmission resonances and nulls due to interference. These resonances and nulls correspond to poles and zeros, with frequency and magnitude determined by the path length differences and splitting ratios of the MZIs and radii and coupling factors of the rings.

A single MZI stage, which consists of two couplers with connecting waveguides of different lengths, introduces a single zero in the complex plane for both the through and cross output ports. Cascading MZI stages introduces additional zeros [4]. MZIs are classified as finite impulse response (FIR) filters as they contain only feedforward paths. Therefore the a coefficients are zero in (2) and (3) and there are no poles present. This limits the crosstalk and passband flatness that can be obtained with MZI filters. Ring resonators, on the other hand, introduce feedback paths and therefore poles, so that the a coefficients are nonzero in (2) and (3). They are classified as infinite impulse response (IIR) filters and usually have better crosstalk and passband flatness than FIR filters. IIR filters usually have longer impulse responses, however. This paper will focus on the magnitude response of the filters, and defer detailed analysis of temporal response to future investigations.

General architectures for arbitrary pole and zero positioning on the complex plane have been proposed in [13] and [14]. These architectures consist of cascaded MZI and ring resonator stages, in which the MZI sections introduce zeros and the ring resonators introduce poles. However, in order to achieve a certain filter response, many stages would need to be cascaded as each stage introduces only one pole and one zero. Coupling ring resonators together, however, results in multiple poles and zeros per resonator, as will be shown in Section III-C and III-D. This reduces the number of ring resonators necessary to achieve a given spectral response. In the following sections, Z-transforms and pole-zero diagrams will be derived for various filters containing ring resonators and coupled ring resonator arrays.

B. Single Ring Resonator Pole-Zero Diagrams

To illustrate pole-zero diagram derivation for ring resonator filters, we first derive the Z-transform for a simple case, a single

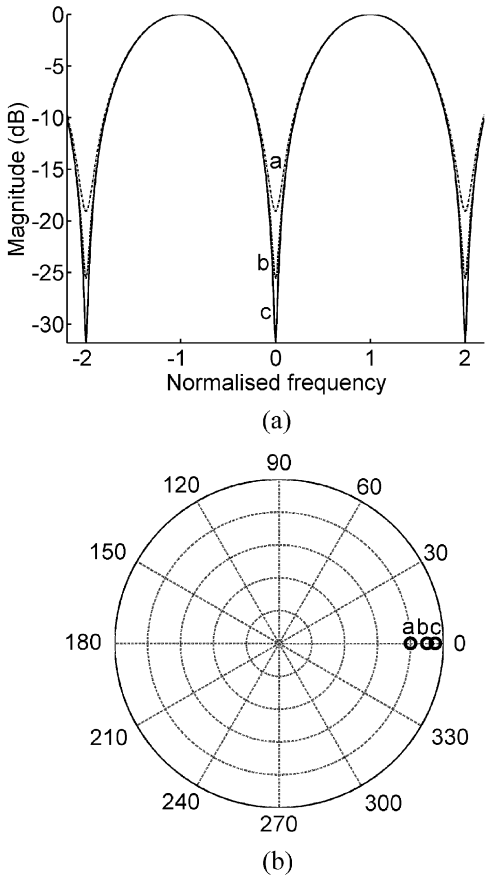

Fig. 1. (a) Magnitude spectra for zeros positioned at various distances from the origin. Curves a, b, and c correspond to zeros at $z = 0.8, 0.9$, and 0.95, respectively. (b) The corresponding pole-zero diagram.

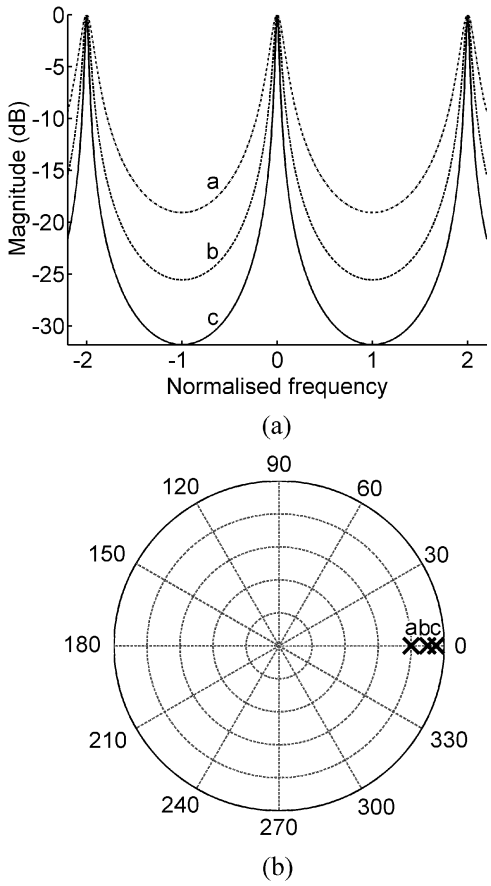

Fig. 2. (a) Magnitude spectra for poles positioned at various distances from the origin. Curves a, b, and c correspond to poles at $z = 0.8, 0.9$, and 0.95, respectively. (b) The corresponding pole-zero diagram.

ring resonator, and follow the procedure given in [4]. The first step is to assign delay terms z^{-1} to the optical waveguide paths in the filter. Fig. 3 shows a schematic of a ring resonator coupled to two straight waveguides. The circumference of the ring resonator corresponds to a unit delay length. A unit delay length is defined as a multiple of the center resonant wavelength of the ring and is represented in the Z-transform as z^{-1}, where $z^{-1} = e^{-\mathrm{i}\omega}$. Here, ω is the normalized frequency equal to $(\Omega - \Omega_{\mathrm{C}})2\pi\mathrm{nR}/\mathrm{c}$, where Ω is the optical frequency, Ω_{C} the center frequency, n the ring effective index, and R the ring radius. To include the effect of power dissipation in the ring, z^{-1} is multiplied by γ, where $(1-\gamma^2)$ is the power attenuation per cycle. Ring waveguide sections corresponding to half the circumference are labeled $\sqrt{\gamma}z^{-1}$ in Fig. 3.

The second step is to determine relations between the signal amplitudes at various points within the filter. These relations include both the delay paths and the matrix equations to describe the directional couplers. As shown in Fig. 3, the signal enters the input port. A portion of this signal is coupled over into the ring at K_1, and a portion passes to the through port. Coupling is usually done using directional couplers, and is described by the following matrix:

$$\Phi_{c1} = \begin{bmatrix} r_1 & -js_1 \\ -js_1 & r_1 \end{bmatrix} \tag{5}$$

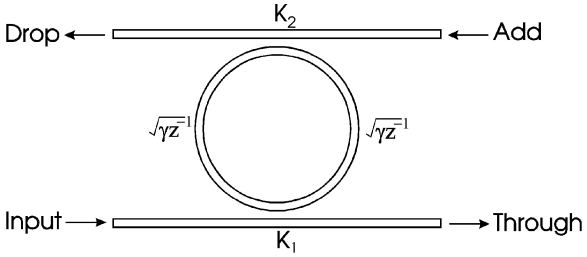

Fig. 3. Schematic of a ring resonator with two directional couplers K_1 and K_2. $\sqrt{\gamma}\mathrm{z}^{-1}$ is the amplitude transmission from one coupler to another via the curved ring waveguide.

where r_1 is the straight-through amplitude coupling factor, s_1 is the crossover coupling factor, and ${s_1}^2 + {r_1}^2 = 1$. There is likewise a second coupler K_2 that allows power to be coupled to the drop port. The signal at this port is the sum of an infinite number of terms

$$S_{\mathrm{drop}} = -s_1 s_2 \sqrt{\gamma z^{-1}}\{1 + r_1 r_2 \gamma z^{-1} + \cdots\} S_{\mathrm{input}}. \tag{6}$$

The first term in the series corresponds to the component of the signal that couples into the ring, traverses half the ring circumference, and couples out again to the drop port. The second term corresponds to that component that undergoes an additional cycle around the ring before coupling to the drop port,

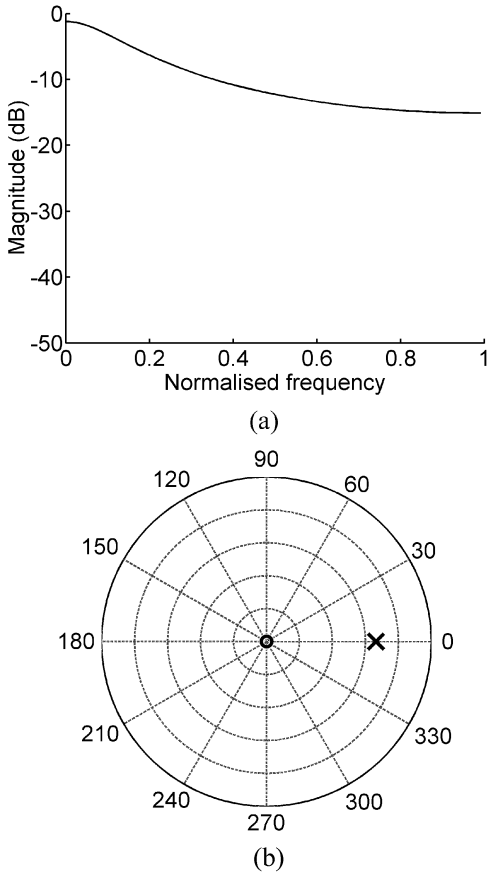

Fig. 4. (a) Magnitude spectrum for the drop port of the single ring-resonator filter shown in Fig. 3. The power coupling factor is 0.7 at both couplers and the power dissipation in the ring is 10% per cycle. (b) The corresponding pole-zero diagram.

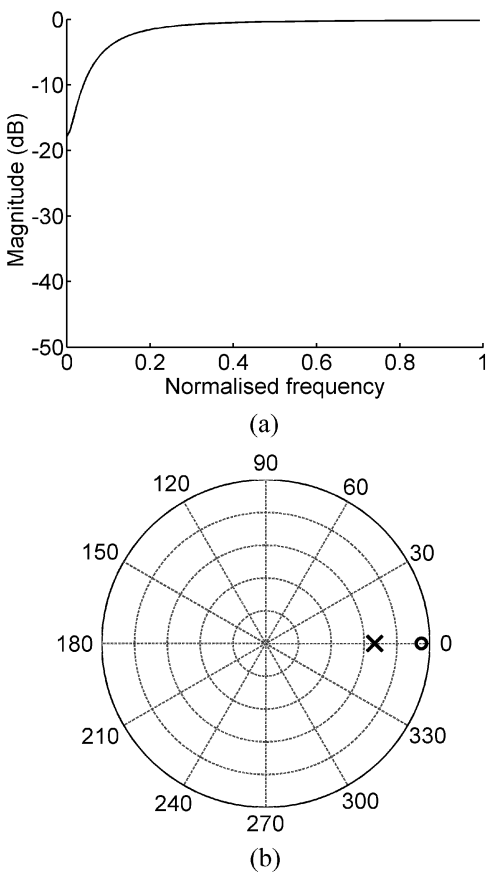

Fig. 5. (a) Magnitude spectrum and (b) pole-zero diagram for the through port of the single ring-resonator filter shown in Fig. 3. The power coupling factor is 0.7 at both couplers and the power dissipation in the ring is 10% per cycle.

and so on for the other terms. Using the Taylor series expansion, the above equation can be simplified to give the drop port transfer function

$$\frac{S_{\text{drop}}}{S_{\text{input}}} = \frac{-s_1 s_2 \sqrt{\gamma} z^{-1}}{1 - r_1 r_2 \gamma z^{-1}}. \tag{7}$$

It can be seen from this equation that there is a single pole at $r_1 r_2 \gamma$. The term $\sqrt{z^{-1}}$ in the numerator results in a zero at the origin, which simply introduces a delay in the overall response but does not affect the spectrum. Fig. 4 shows the magnitude spectrum and pole-zero diagram for a power coupling factor of 0.7 at both couplers, and power dissipation in the ring of 10% per cycle. Note that since the signal is periodic and symmetrical, only half of the FSR is plotted in Fig. 4.

The through port transfer function is likewise given by

$$\frac{S_{\text{through}}}{S_{\text{input}}} = \frac{r_1 - r_2 \gamma z^{-1}}{1 - r_1 r_2 \gamma z^{-1}}. \tag{8}$$

It is evident from this equation that there is a pole at the same location as in the through port signal and a zero at $r_2\gamma/r_1$. Fig. 5 shows the resulting magnitude spectrum and pole-zero diagram.

C. Z-Transforms for Various Ring Resonator Filters

We shall study several types of ring resonator-based filters using pole-zero diagrams. In order to produce these diagrams, however, we must first determine the Z-transforms for each filter.

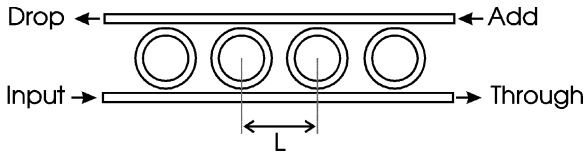

Fig. 6. Schematic of a parallel-coupled ring resonator filter.

To illustrate the process of finding the Z-transform for coupled ring resonator filters, we shall now derive the Z-transform for parallel-coupled ring-resonator arrays. Fig. 6 shows a schematic of this filter. As before, the first step is to assign delay terms to the various optical waveguide paths in the filter. The circumference of the rings was assigned a delay of z^{-1}. Also, the spacing between the rings L was chosen such that $z^{-1/2} = e^{-\beta L}$, where β is the bus propagation constant. This ensures a periodic spectral response suitable for a wavelength interleaver. [15]

The next step is to determine the relations between the signal amplitudes at various points in the filter. The transfer functions of a single ring resonator have already been derived, and so we can write the transfer matrix of a single ring resonator as

$$\begin{bmatrix} S_{\text{input}} \\ S_{\text{drop}} \end{bmatrix} = \begin{bmatrix} T_{11} & T_{12} \\ T_{21} & T_{22} \end{bmatrix} \begin{bmatrix} S_{\text{through}} \\ S_{\text{add}} \end{bmatrix} = T_1 \begin{bmatrix} S_{\text{through}} \\ S_{\text{add}} \end{bmatrix} \tag{9}$$

where

$$T_{11} = \frac{1 - r_1 r_2 \gamma z^{-1}}{r_1 - r_2 \gamma z^{-1}}$$
$$T_{12} = -T_{21} = \frac{s_1 s_2 \sqrt{\gamma z^{-1}}}{r_1 - r_2 \gamma z^{-1}}$$
$$T_{22} = \frac{r_1 r_2 - \gamma z^{-1}}{r_1 - r_2 \gamma z^{-1}}. \quad (10)$$

In this equation, S_{input}, S_{drop}, S_{through}, and S_{add} correspond to the signals at the ports labeled in Fig. 3. The transfer matrix of the straight waveguide segments T_ϕ is given by

$$T_\phi = \begin{bmatrix} \sqrt{z} & 0 \\ 0 & \sqrt{z^{-1}} \end{bmatrix}. \quad (11)$$

Now we must determine the overall filter response. To do this we use the transfer matrix method outlined in [16]; however, we substitute z^{-1} for $e^{-i\omega}$. To obtain the transfer matrix of an N-coupled array, the matrices for each ring and the connecting straight waveguide segments are multiplied together

$$\begin{bmatrix} S^1_{\text{input}} \\ S^1_{\text{drop}} \end{bmatrix} = T_1 \cdot T_\phi \cdot T_2 \cdot T_\phi \cdots T_N \begin{bmatrix} S^N_{\text{through}} \\ S^N_{\text{add}} \end{bmatrix} = M \begin{bmatrix} S^N_{\text{through}} \\ S^N_{\text{add}} \end{bmatrix}. \quad (12)$$

The drop port signal is calculated from matrix M as ${S^1}_{\text{drop}}/{S^1}_{\text{input}} = M_{21}/M_{11}$ and the through port signal as ${S^N}_{\text{through}}/{S^1}_{\text{input}} = 1/M_{11}$ by setting the signal from the add port ${S^N}_{\text{add}}$ to zero. Note that in this paper, all signals are referred to the input port. The equations for the drop and through port signals can be put into the form of (4). That is, the numerator and denominator terms can be factored to find the zeros and poles, respectively. The final equations depend on the number of rings in the array. We shall not present them here since they are quite long, and pole-zero diagrams can be used to clearly summarize the information contained in these equations.

The above example illustrates the method for determining the Z-transforms and pole-zero diagrams of an array of coupled ring resonators. The Z-transforms of the MZI with ring resonator and the series-coupled ring array are derived in [4].

We calculated the Z-transforms of various filter structures using Mathematica to multiply the matrices and perform symbolic manipulations to simplify the equations. This method is more accurate than substituting numerical values before multiplying the matrices. Putting the equations in the form of (3) allowed the a and b coefficients to be easily determined. These coefficients were imported into Matlab to enable plotting of pole-zero positions and other standard signal-processing routines to be done. It was thus not necessary to factor the equations in Mathematica to find the poles and zeros.

In summary, the process of determining the pole-zero diagrams for optical filters is as follows.

1) Assign delay terms z^{-1} to optical paths in the filters.
2) Find equations relating the signal amplitudes between various points in the filter array.
3) Calculate the overall filter response (Z-transform) for each output port using matrix multiplication.
4) Put the resulting equations in a form suitable for determining the poles and zeros.

III. Pole-Zero Diagrams for Wavelength Interleaver Filters

In this section, we work out pole-zero diagrams for several different filter types for wavelength interleaving. This will illustrate several uses of pole-zero diagrams, including selection of the most suitable filter structure for a given application, graphical optimization, and synthesis of new filters by superimposing pole-zero diagrams.

A. Target Filter Response

The performance requirements of interleaving filters with 50-GHz channel spacing includes low insertion loss (<1 dB), low crosstalk (<23 dB), and box-like passband shape, among other things [15]. We designed a minimum order filter using the filter design and analysis tool in Matlab. This filter has the least number of poles and zeros necessary to meet the above performance requirements, and they are optimally located to achieve minimum crosstalk. We designate this filter as the "target" filter.

An IIR Chebyshev type II was chosen since it is free of passband ripple. The −3 dB passband width was set as 50% of the FSR, and the stopband frequency was set as 80% of the FSR. We defined crosstalk as the maximum value of the filter magnitude response in the stopband. We varied the crosstalk, and Matlab produced minimum-order filter designs that satisfied these crosstalk levels.

It was found that for crosstalk higher than −26 dB, the resulting filter design was second order. For values between −26 and −40 dB, the filter was third order, and for crosstalk lower than −40 dB the filter was fourth order. Since a second-order filter can barely satisfy the crosstalk requirements of an interleaver, a third-order filter was selected. A fourth-order filter would introduce unnecessary complexity, since a third-order filter has sufficient crosstalk performance. Fig. 7 shows the target filter response in the drop port of an interleaver. An interleaver ideally has symmetrical response in the drop and through ports, and the corresponding pole-zero plots are likewise symmetrical. The through port spectrum is identical to the drop port's, but shifted by half the FSR. The poles and zeros for the through port are obtained by reflecting the poles and zeros of the drop port about the imaginary axis. To save space, the through port diagrams are not shown.

In Fig. 7, it can be seen that there are three zeros at roughly 148°, 180°, and 212°. The zeros at 148° and 212° are complementary pairs, and the first of these is responsible for the null in the magnitude spectrum at a normalized frequency value of 0.82. The zero at 180° is responsible for the transmission null at a frequency of one. There are three poles. The pole near the origin can be ignored, as its close proximity to the origin implies that it has little influence on the magnitude response. The other two poles at 90° and 270°, however, result in improved passband flatness. It is also evident from Fig. 7(a) that the crosstalk is −40 dB, the best that can be attained with a third-order filter for the given bandwidth. Subsequently, we refer to the position of the poles and zeros of this third-order Chebyshev filter, shown in Fig. 7(b), as the target positions.

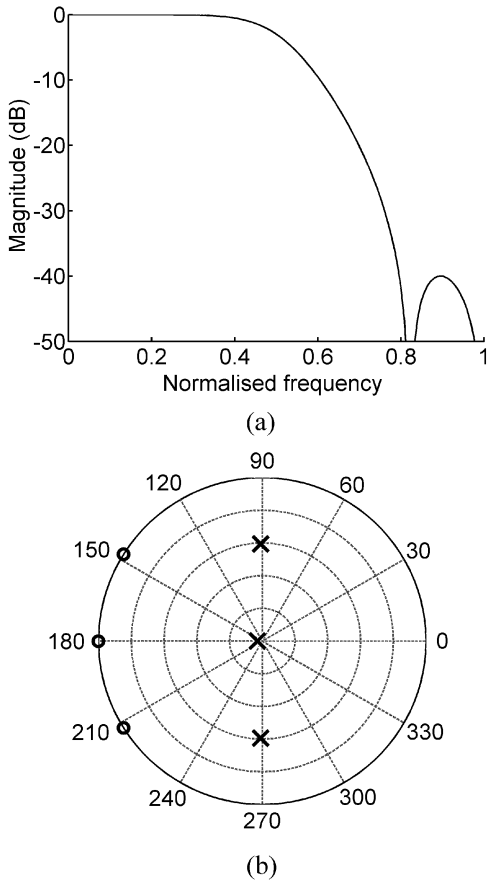

Fig. 7. (a) Target filter magnitude response and (b) the corresponding pole-zero diagram for the drop port. This filter is third-order Chebyshev type II, with -3 dB passband width equal to 50% of the FSR and stopband frequency equal to 80% of the FSR. Crosstalk is -40 dB.

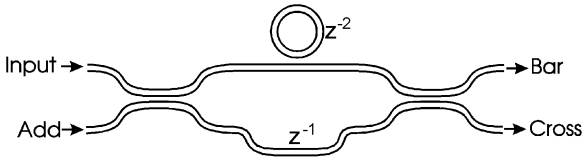

Fig. 8. Schematic of a filter consisting of a ring resonator coupled to one arm of an MZI. The delay in the through arm is z^{-1}, and the delay in the ring resonator is z^{-2}.

In order to characterize the passband flatness we define a shape factor as the -1 dB bandwidth divided by the -10 dB bandwidth. For the case of the target filter, in Fig. 7(a), this is 0.78. A higher shape factor implies a more box-like spectrum.

Although this paper concerns tailoring of filter magnitude response, we note that poles and zeros significantly influence the wavelength dispersion and group delay of filters and refer the reader to [4] for details. Dispersion introduces an additional constraint on pole and zero positions, since acceptable dispersion requires that there be no poles or zeros in the vicinity of the passband. The dispersion of commercial interleaver devices with 50-GHz channel spacing is typically less than ± 30 ps/nm over a ± 10-GHz passband width. For the target device, assuming 50-GHz channel spacing, we calculated a dispersion of around ± 50 ps/nm over this passband for both output ports. Referring to the pole-zero diagram for the drop port [Fig. 7(b)], if the circumference corresponds to an FSR of 100 GHz, then a ± 10 GHz passband corresponds to the region between 36° and 324°. The dispersion in this passband is mainly influenced by the two poles at 90° and 270°, since they are closer to the passband than the zeros.

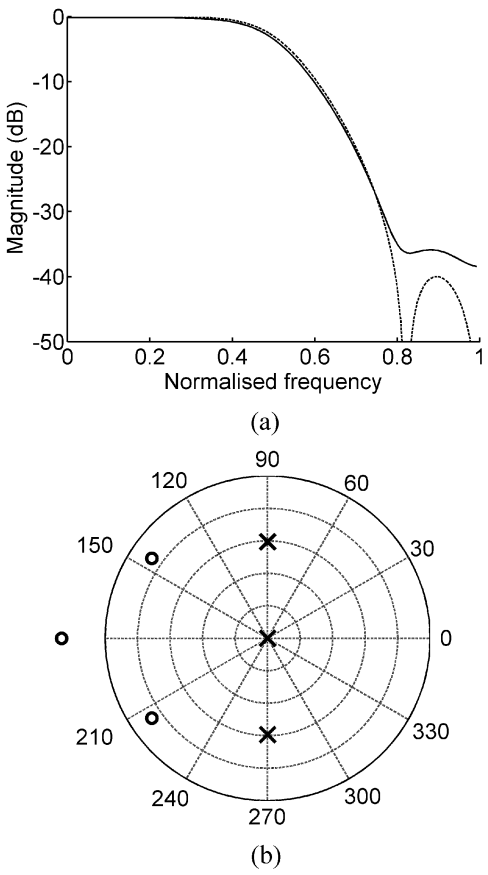

Fig. 9. (a) Magnitude response (solid line) and (b) pole-zero diagram for the MZI/ring resonator filter illustrated in Fig. 8. The splitting factor of the couplers is 50:50. The coupling factor of the ring resonator to the straight waveguide is 86.2%, and the power loss per cycle in the ring is 10%. The dashed line in (a) corresponds to the response of the target filter in Fig. 7(a) and is shown for reference.

B. MZI Containing Ring Resonator

An MZI containing a ring resonator is illustrated in Fig. 8. It can operate as a deinterleaver, splitting channels at the input port and sending the odd channels to the cross port and the even channels to the bar port. In addition, the filter can operate as an interleaver, combining wavelength signals from the add and input ports. Fig. 9 shows the pole-zero diagrams and spectral response for the cross port. The bar port is identical but shifted in frequency by half the FSR. This filter is discussed in detail in [4] and [12].

The splitting factor of the MZI was set to 50:50, and a power loss of 10% per cycle assumed for the ring resonator. Crosstalk was found to be minimal at a ring resonator coupling power coupling ratio of 86.2%. As can be seen, the pole positions correspond closely to the target positions of the Chebyshev filter; however, the zeros have moved away from the unit circle due to loss. When loss is removed the zeros move back to their optimal target locations, and the pole-zero diagram becomes iden-

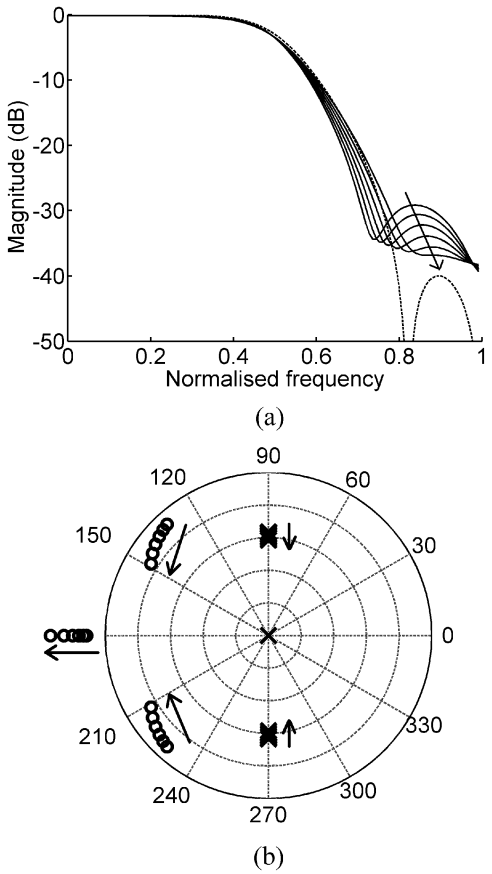

Fig. 10. (a) Magnitude spectrum and (b) pole zero diagram for the MZI/ring resonator filter with varying coupling ratio between the ring and straight waveguide. Power coupling is varied from 0.82 to 0.87 in steps of 0.01, and the arrows indicate the movement of the curves and pole-zero positions as this ratio increases.

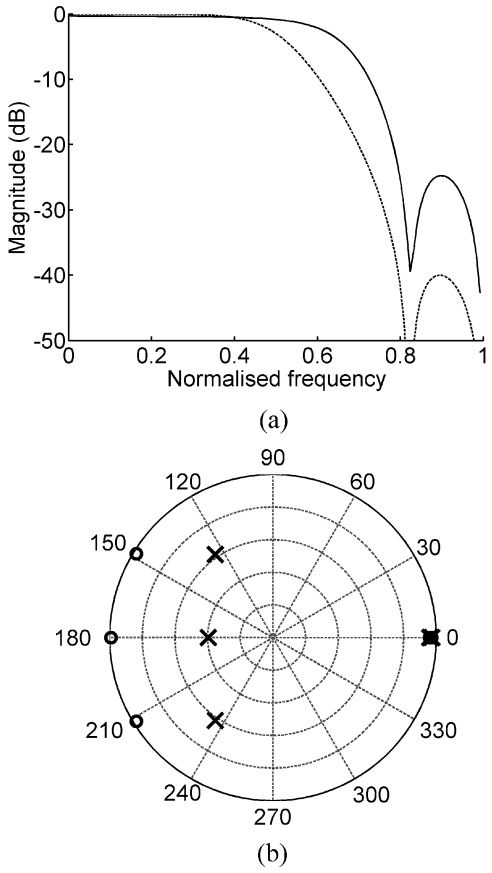

Fig. 11. (a) Magnitude spectrum and (b) pole-zero diagram for the drop port of the four-ring parallel-coupled ring resonator array illustrated in Fig. 6. The coupling prefactor is 0.7 and the apodization 0.125.

tical to Fig. 7(b). Fig. 9 shows that loss diminishes the effect of the zeros, causing the sidelobe to increase in magnitude and broaden.

Fig. 10 illustrates the effect of changing the ring power coupling ratio. In this figure, the arrows indicate the directions that the poles or zeros move as the coupling ratio is increased. In Fig. 10 the coupling ratio increases from 0.82 to 0.87 in steps of 0.01, and as it does so the zero at 180° moves away from the unit circle, so that the effect of this zero on the shape of the spectral response diminishes. The other zeros move toward the real axis and away from the unit circle. Both of these changes are reflected in the magnitude spectrum [Fig. 10(a)]. The poles move only slightly as power coupling changes.

It is interesting to observe from these diagrams that crosstalk is lowest when the zeros are closest to their target positions. Therefore, optimization of the power coupling ratio can be done simply by varying this parameter while observing both the pole-zero and magnitude spectrum diagrams. Optimal crosstalk is obtained when the pole and zero positions most closely approximate their target positions. In particular, the zeros predominately determine the crosstalk. This example suggests a useful graphical optimization technique of adjusting parameters in order to match pole and zero positions to their target locations.

C. Four-Ring Parallel-Coupled Ring Resonator Array

Pole-zero diagrams were found for parallel-coupled ring resonator arrays with various numbers of rings. It was found that the pole-zero diagram for a four-ring array best approximates the target case, as we will show. The four-ring parallel-coupled array is illustrated in Fig. 6. This filter can operate as a deinterleaver, sending odd channels to the drop port and even channels to the through port. It can also operate as an interleaver, combining channels from the input and add ports and sending the combined signal to the through port.

The procedure used to optimize the coupling coefficients between the rings and the straight waveguides [15] is summarized here. The coupling is exponentially apodised, according to $\kappa_{\mathrm{N}} = A\,\mathrm{Exp}[-a_p(N - N_{\mathrm{c}})^2]$, where N is the ring number, N_{c} is equal to half the total number of rings, A is the coupling prefactor, and a_p is the apodization coefficient. The input and output ring-bus coupling coefficients are equal. Optimization of the output spectra was done by varying A and a_p by small increments and calculating the crosstalk in the drop and through ports for each parameter combination. The optimum was achieved when the crosstalk levels in both output ports were a minimum. The optimal values of the coupling prefactor and apodization were 0.7 and 0.125, respectively.

Fig. 11 shows that in the drop port pole-zero diagram, as for the target case, there is a zero at 180° and zeros at around 148°

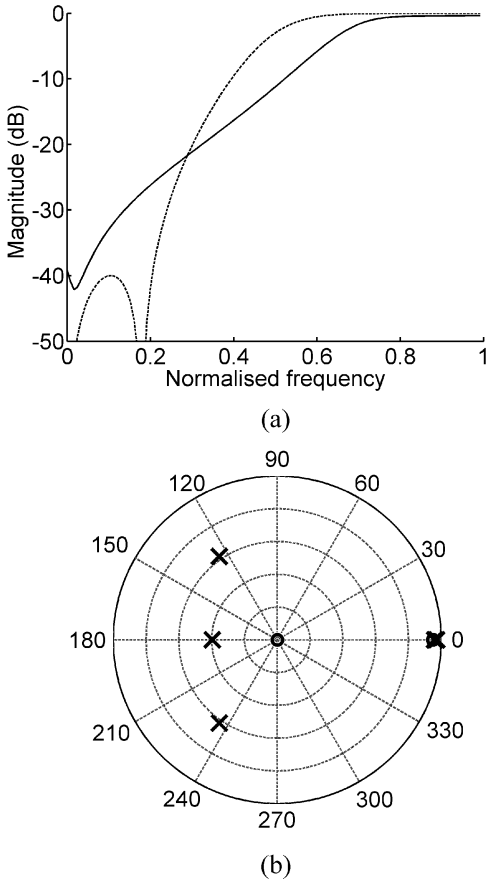

Fig. 12. (a) Magnitude spectrum and (b) pole zero diagram for the through port of the four-ring parallel-coupled ring resonator array illustrated in Fig. 6. The coupling prefactor is 0.7 and the apodization 0.125.

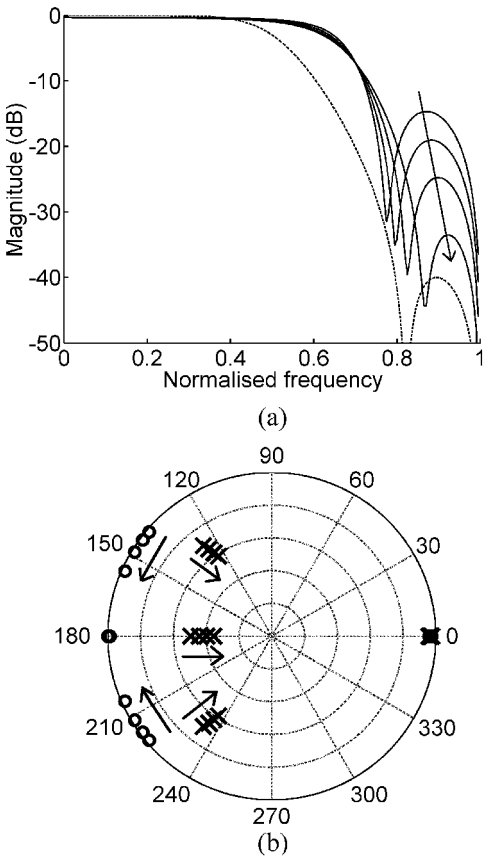

Fig. 13. (a) Magnitude spectrum and (b) pole zero diagram for the drop port of the four-ring parallel-coupled ring resonator filter for variable apodization. Apodization is increased from 0.075 to 0.15 in steps of 0.025, with coupling prefactor fixed at 0.7 and the loss in the ring set to 10%. Arrows indicate the direction of increasing apodization.

and 212°. The drop port of the parallel-coupled ring array differs from the target case in two regards. First, it is evident that there are three poles in the negative real plane, whereas for the target design they are positioned on the imaginary axis. Secondly, there are three poles and three zeros overlapping at a position close to $z = 1$. Since they overlap, the resulting magnitude spectrum is flat at the center frequency.

The pole-zero diagram and magnitude spectrum of the through port differs considerably from the target case for this type of filter, as Fig. 12 shows. There are four zeros and three poles at close to $z = 1$, and so there is one extra zero at this point. There are no zeros at 32° or 328°, and so the shape of the magnitude spectrum is significantly different for this port compared to the target case. Also, the pole positions are the same as for the drop port. However, since the poles have moved away from the imaginary axis, the shape factor is degraded. It can be seen that the spectrum is far from the target case due to the different number of zeros and different positioning of the poles. The utility of pole-zero diagrams for filter design is evident. Since the number of zeros does not correspond to the target case, it is impossible to attain the crosstalk levels and passband shape required by simply adjusting parameters. This is not evident from looking at the magnitude spectrum alone.

We now examine pole and zero dynamics for this filter. First, apodization is varied, as shown in Fig. 13. Apodization increases from 0.075 to 0.15 in steps of 0.025, with coupling prefactor fixed at 0.7. The arrows indicate the directions that the poles and zeros and magnitude spectrum move as apodization increases. It is clear that the pole and zero positions cannot be adjusted independently, as both move simultaneously when the apodization parameter is varied. It can also be seen that the zeros overlap the target positions at around 148° and 212° for an apodization of 0.0125. This in fact corresponds to a minimum in the crosstalk versus apodization. This is similar to the case for the MZI with ring resonator in that optimal crosstalk was attained with zeros closest to the target positions. For larger apodization, the sidelobe is smaller but the main peak is broader, increasing crosstalk. For smaller apodization, crosstalk is higher due to a larger sidelobe. The pole positions change slightly but have a minor impact on the drop port spectrum. The crosstalk in the through port spectrum is determined mainly by the poles, as shown in Fig. 14. As apodization increases, the poles move away from the unit circle and crosstalk so increases.

We now consider pole and zero dynamics as the coupling prefactor is varied. Fig. 15 shows the effect on the drop port of increasing the coupling prefactor from 0.3 to 0.8 in steps of 0.1. As the coupling prefactor increases, the main peak in the drop port spectrum becomes broader. The sidelobe height initially increases and then decreases. As before, the lowest crosstalk occurs if the zeros are at their target locations. In the through port (not shown), a higher prefactor decreases crosstalk, at the ex-

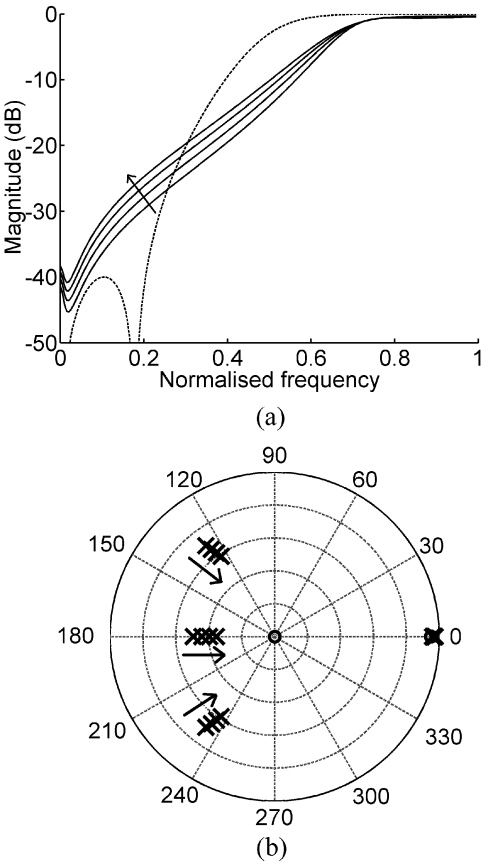

Fig. 14. (a) Magnitude spectrum and (b) pole zero diagram for the through port of the four-ring parallel-coupled ring resonator filter for variable apodization. Parameters are those used in Fig. 13. Arrows indicate the direction of increasing apodization.

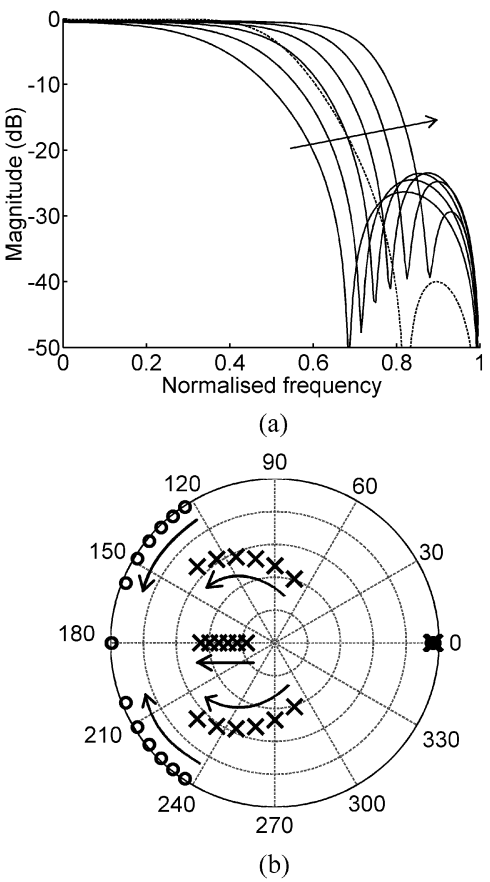

Fig. 15. (a) Magnitude spectrum and (b) pole zero diagram for the drop port of the four-ring parallel-coupled ring resonator filter for coupling prefactor varying from 0.3 to 0.8 in steps of 0.1. Arrows indicate the direction of increasing prefactor. The apodization is set to 0.125 and the loss per cycle in the ring is set to 10%.

pense of a much narrower passband. Although lower crosstalk in the drop port is obtained with lower prefactor, this compromises crosstalk in the throughport. Thus, when varying parameters such as prefactor, crosstalk in both the through and drop ports must be considered, as they are interrelated via their dependence on those parameters.

When obtaining the optimum values of the prefactor and apodization parameters, it should be realized that the parameter values for which the zero positions correspond to their target positions are not unique. However, the parameter values for which crosstalk in the through and drop ports are equal are unique in this example. The utility of the pole-zero diagrams is that it allows optimization of parameter values by graphically locating zeros at their target positions. It is only necessary to check from the magnitude spectrum graphs whether the crosstalk levels in the drop and through ports are equal for parameter combinations with correctly positioned zeros.

We now remark on the dispersion of this filter. Looking at Fig. 11(b), it can be seen that for the drop port the poles are well away from the passband, which is between 36° and 324°. The calculated dispersion of ± 12 ps/nm is therefore acceptably small. However, as Fig. 12(b) shows for the through port, the poles are closer to the passband region between 144° and 216°. The dispersion in the passband for this port is therefore very high, around ± 110 ps/nm.

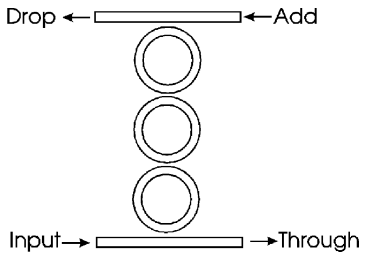

Fig. 16. Schematic of a filter with three ring resonators coupled in series.

D. Three-Ring Series-Coupled Ring Resonator Array

A series-coupled ring resonator array with three rings is illustrated in Fig. 16. Fig. 17 shows the through port pole-zero diagram and magnitude spectrum for this filter. The ring–ring power-coupling coefficients were 0.39, the ring–straight waveguide-coupling coefficients were 0.80, and power dissipation in each ring was 10%. The drop port spectrum is not shown. For the drop port there are only poles, and so there is a poor match between the magnitude spectrum of this filter and the target filter spectrum. The through port, on the other hand, has three zeros closely matching the target positions. Although the poles are not ideally positioned, the zeros dominate the spectrum. A good

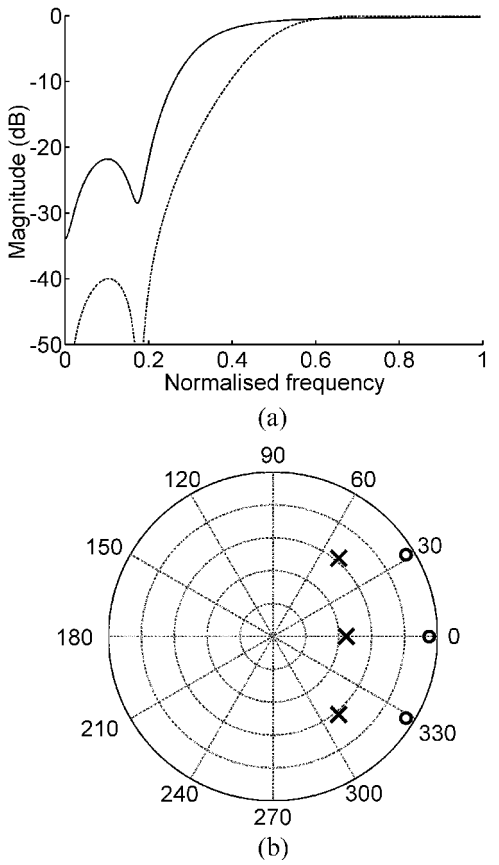

Fig. 17. (a) Magnitude spectrum and (b) pole-zero diagram for the through port of the three-ring series-coupled ring resonator array illustrated in Fig. 16. The ring–ring power-coupling coefficients are 0.39 and the ring–straight waveguide-coupling coefficients are 0.80. Power loss per cycle in each ring is 10%.

match between the through port and target spectrum can therefore be obtained, and we use this to produce a new filter design in the next section.

E. Filter With Parallel-Coupled and Series-Coupled Ring Array Stages

Cascading filters is equivalent to superimposing their pole-zero diagrams if no new feedback paths are created. This is because the transfer functions of two filters are simply multiplied together. For example, if the output signal from a filter is sent to a ring resonator, the signal at the drop port of the ring will have a pole-zero diagram consisting of poles and zeros from the first filter plus poles and zeros from the drop port transfer function of the ring.

This convenient feature of pole-zero diagrams can be exploited to design filters. For example, Fig. 11 shows that the drop port of the parallel-coupled array with four rings has the correct number of zeros in the desired locations. The through port, however, has a far from optimal pole-zero diagram, as there is only one zero responsible for the transmission null in the spectrum, as Fig. 12 shows. Therefore, the output from this port must be modified by adding two zeros, one at 32° and another at 328°. Inspection of Fig. 17 shows that the through port of the three-ring series-coupled array has the desired zeros. Therefore, superimposing the four-ring parallel and three-ring

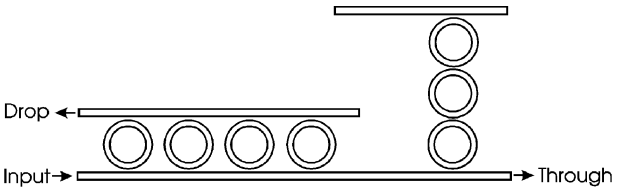

Fig. 18. Schematic of a new ring resonator filter design consisting of a three-ring series filter coupled to the through port of a four-ring parallel filter.

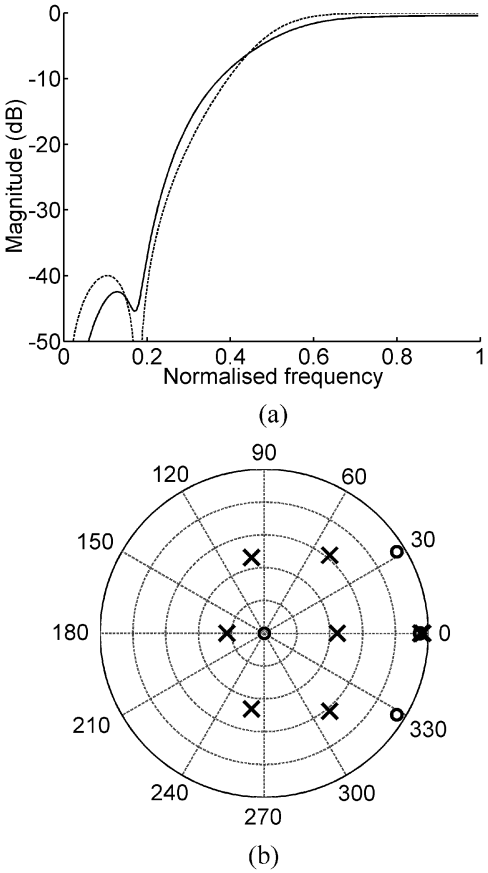

Fig. 19. (a) Magnitude spectrum and (b) pole-zero diagram for the through port of the filter illustrated in Fig. 18. For the parallel stage, the optimal coupling prefactor was 0.5 and the optimal apodization was 0.176. For the series stage, the ring–straight waveguide coupling was 0.8 and the ring–ring coupling was 0.39.

series array through port pole-zero diagrams should result in a filter with a magnitude spectrum close to the target spectrum. That is, the through port should have zeros at 0°, 32°, and 328°, and the drop port should have zeros symmetrically located at 180°, 148°, and 212°. Fig. 18 shows how the filters should be connected for operation as a deinterleaver. Note that for this filter to operate as an interleaver, the odd and even channels should be sent to the drop and through ports, respectively, and the combined signal will emerge from the input port.

The resulting pole-zero and magnitude spectrum diagrams for the through port are shown in Fig. 19. It is evident that this filter provides close to the target transfer characteristics in this port. The drop port is not shown; however, its spectrum is similar. The crosstalk in the through port is −37 dB, and the crosstalk in the drop port is −35 dB. The dispersion for both output ports is imporoved over the target case, around ±25 ps/nm.

This filter design was obtained by superimposing the pole-zero diagrams of the parallel-coupled and series-coupled through ports in order to obtain a pole-zero diagram close to that for the target filter. This design would not have been apparent without pole-zero diagrams to visualize the spectral characteristics of the filters. Simply comparing the magnitude spectra of filters is insufficient for estimating the spectra that result when those filters are cascaded. This example, therefore, illustrates clearly the utility of pole-zero diagrams for optical filter design.

F. Summary of the Application of Pole-Zero Diagrams to Optical Filter Design

In this section we summarize our approach to designing optical filters using ring resonators and MZI structures, as illustrated in the previous sections.

In order to design a filter, it is useful to first produce a pole-zero diagram for a classical filter, such as a Chebyshev filter. The poles and zeros for this filter are optimally located according to given design criteria, and serve as a target for optimization of an actual filter structure. This target filter design does not correspond to any particular physical structure. Its purpose is to determine the best performance that is achievable with a filter of a given order. If a specific value of crosstalk is required, for example, then a classical filter can be designed with crosstalk equal to or exceeding that specification with a minimal number of poles and zeros. Minimization of filter order is important since it simplifies filter design, allowing fewer MZI and ring resonator stages to be used.

Pole-zero diagrams are useful for determining whether a given filter structure can attain desired levels of performance, in the sense of matching the spectrum of a classical filter design. If the pole and zero positions cannot be made to overlap the positions for a target filter, then performance will be less than optimal. Additional poles and zeros may also be present, which can cause undesirable features in the spectrum. Also, poles and zeros may be missing at certain points. By comparing the pole-zero diagrams for a filter structure with the diagrams for a target filter, the usefulness of a filter structure for a given application can be quickly assessed. Furthermore, pole-zero diagrams for different filter structures can be compared to see which offer superior performance. For the interleaver example in this paper it is clear that the poles and zeros of the filter with an MZI coupled to a ring resonator more closely match those of the target filter than either the series or parallel-coupled arrays. This filter therefore has a spectral response closer to the target response.

Pole and zero dynamics, or the behavior of poles and zeros as parameters are varied, can be visualized easily using pole-zero diagrams. This has several applications. First, by varying parameters over a wide range, the full extent of pole and zero positions can be seen and compared to the target pole and zero positions, as in Figs. 13–15. This helps in determining whether a filter can potentially offer good spectral characteristics. Secondly, parameter values can be optimized by adjusting the parameters until overlap of the poles and zeros with their target positions occurs. Note that in this case pole-zero diagrams provide a rough visual guide for optimization, and the magnitude spectrum must be concurrently monitored as parameters are adjusted. This method, however, can be applied to any filter structure and avoids the difficulty of deriving filter synthesis algorithms.

Finally, pole-zero diagrams can be superimposed by cascading filter structures to achieve a desired filter response function, as when we added a series-coupled ring array to the through port of a parallel-coupled ring array. This is not possible by simply observing the magnitude spectrum of each filter and illustrates clearly the utility of pole-zero diagrams.

IV. Conclusion

In this paper, we proposed the application of pole-zero diagrams to the design of ring resonator-based filters for photonics applications. We studied optical filter structures consisting of ring resonators as well as MZIs using pole-zero diagrams. We showed that pole-zero diagrams provide additional and important information for obtaining optimal photonic filter designs. This information cannot be provided by conventional methods that concern mainly spectral characteristics. We proposed new methods for optimization and summarized guidelines for their use in photonic filter design. Further, we proposed a new filter structure for wavelength interleaving and deinterleaving consisting of parallel and series-coupled filter array stages. This filter structure was obtained by studying pole-zero diagrams, demonstrating that pole-zero diagrams can be very useful for photonic filter design.

References

[1] Y. Yanagase, S. Suzuki, T. Kokubun, and S. T. Chu, "Vertical triple series-coupled microring resonator filter for passband flattening and expansion of free spectral range," *Jpn. J. Appl. Phys.*, vol. 41, no. 2A, pp. L141–L143, 2002.

[2] C. Ozturk, A. Huntington, A. Aydinli, Y. T. Byun, and N. Dagli, "Filtering characteristics of hybrid integrated polymer and compound semiconductor waveguides," *J. Lightwave Technol.*, vol. 20, pp. 1530–1536, Aug. 2002.

[3] F. C. Blom, D. R. van Dijk, H. J. W. M. Hoesktra, A. Driessen, and T. J. A. Popma, "Experimental study of integrated-optics microcavity resonators: toward an all-optical switching device," *Appl. Phys. Lett.*, vol. 71, no. 6, pp. 747–749, 1997.

[4] C. K. Madsen and J. H. Zhao, *Optical Filter Design and Analysis: A Signal Processing Approach*. New York: Wiley, 1999.

[5] A. V. Oppenheim and R. W. Schafer, *Discrete-Time Signal Processing*. Englewood Cliffs, NJ: Prentice-Hall, 1989.

[6] J. Azana and L. R. Chen, "Multiwavelength optical signal processing using multistage ring resonators," *IEEE Photon. Technol. Lett.*, vol. 14, pp. 654–656, May 2002.

[7] L. N. Binh, N. X. Thien, and N. Q. Ngo, "Realization of Butterworth-type optical filters using 3×3 coupler ring resonators," *Proc. Inst. Elect. Eng. Optoelectron.*, vol. 143, no. 2, pp. 126–134, 1996.

[8] E. M. Dowling and D. L. MacFarlane, "Lightwave lattice filters for optically multiplexed communication systems," *J. Lightwave Technol.*, vol. 12, pp. 471–486, Mar. 1994.

[9] L. N. Binh, N. Q. Ngo, and S. F. Luk, "Graphical representation and analysis of the Z-shaped double-coupler optical resonator," *J. Lightwave Technol.*, vol. 11, pp. 1782–1792, Nov. 1993.

[10] M. Oguma, T. Kitoh, Y. Inoue, T. Mizuno, T. Shibata, M. Kohtoku, and Y. Hibino, "Compactly folded waveguide-type interleave filter with stabilized couplers," in *Proc. Optical Fiber Telecommunications Conf. 2002*, 2002, pp. 70–72.

[11] A. Melloni, "Synthesis of a parallel-coupled ring-resonator filter," *Opt. Lett.*, vol. 26, no. 12, pp. 917–919, 2001.

[12] R. Harbers, "A passband-flattened integrated optical wavelength filter," M.S. thesis, Faculty of Applied Physics, University of Twente, the Netherlands, 2001.

[13] K. Junguji, "Synthesis of coherent two-port optical delay-line circuit with ring waveguides," *J. Lightwave Technol.*, vol. 14, pp. 1882–1898, Aug. 1996.
[14] C. K. Madsen, "Efficient architectures for exactly realizing optical filters with optimum bandpass designs," *IEEE Photon. Technol. Lett.*, vol. 10, pp. 1136–1138, Aug. 1998.
[15] C. J. Kaalund, Z. Jin, W. Li, and G. D. Peng, "Novel optical wavelength interleaver based on symmetrically parallel-coupled and apodized ring resonator arrays," presented at the SPIE's 48th Annu. Meeting: Int. Symp. Optical Science and Technology, San Diego, CA, Aug. 2003.
[16] R. Grover, V. Van, T. A. Ibrahim, P. P. Absil, L. C. Calhoun, F. G. Johnson, J. V. Hryniewicz, and P.-T. Ho, "Parallel-cascaded semiconductor microring resonators for high-order and wide FSR filters," *J. Lightwave Technol.*, vol. 20, pp. 900–905, May 2002.

Christopher J. Kaalund, photograph and biography not available at the time of publication.

Gang-Ding Peng, photograph and biography not available at the time of publication.